Kr and ^{4}He Adsorption on Individual Suspended Single-Walled Carbon Nanotubes

**Hao-Chun Lee · Oscar E. Vilches · Zenghui Wang ·
Erik Fredrickson · Peter Morse · Richard Roy ·
Boris Dzyubenko · David H. Cobden**

Abstract We report mass and conductance adsorption isotherms of Kr on individual, single-walled, suspended carbon nanotubes for 53 K < T < 90 K for several devices, and of ^{4}He for 5 K < T < 8 K for two devices. Different nanotubes, probably of different diameter and/or chirality, yield different phase diagrams, full monolayer coverages, and partial wetting characteristics for Kr. The ^{4}He results show, for one of the devices, a greatly reduced heat of adsorption as compared to the well studied system of ^{4}He on graphite.

1 Introduction

Volumetric adsorption isotherms of rare gases on uniform substrates of relatively large area per unit volume have yielded a large body of knowledge on the phases and phase transitions of a single layer of atoms as a function of their surface density. Several books [1–3] have been published on this subject. Mass adsorption isotherms on Au, Ag, and many alkali metals have also been widely studied by the use of quartz microbalances; here the adsorption area, a few square millimeters, consists of two metal electrodes on each side of a thinly cut quartz crystal [4–7]. Mass adsorption measurements on a suspended graphite fiber have produced reliable isotherms on a small-area substrate [8]. Recently we reported the first quantitative measurements of mass adsorption of Kr and Ar on the surface of an individual, suspended single wall

H.-C. Lee · O.E. Vilches (✉) · Z. Wang · E. Fredrickson · P. Morse · R. Roy · B. Dzyubenko ·
D.H. Cobden
Department of Physics, University of Washington, Seattle, WA 98195-1560, USA
e-mail: lowtemp@u.washington.edu

carbon nanotube [9]. For a nanotube 1.5 μm long and 2 nm in diameter the adsorption area is about 10^{-14} m^2 and one completed monolayer of Kr at the surface density observed when adsorbed on graphite ($\approx$0.071 atoms/Å^{-2}) has about 70,000 atoms. The sensitivity of the resonance frequency measurements is in the range of a few atoms, although our measurements usually have lower resolution due to the need to obtain complete isotherms in a reasonable time.

In this article we report measurements of the adsorption of Kr on several different nanotube devices, and of ^{4}He on two devices. These measurements give a good indication of what can be obtained from the resonance frequency technique. In addition, we observe small changes in the electrical conductance of some of the nanotubes with the density of the physisorbed layer, which have allowed us to observe sudden changes of phase of the Kr monolayer at constant temperature [9]. This article has a brief review of the experimental methods, followed by a description and discussion of the Kr results. The rather preliminary measurements of adsorption of ^{4}He were done measuring frequency in one device and conductance in the other. From the data, we calculate the Kr isosteric heat of adsorption per atom, Q_{st} (in units of equivalent temperature, K), for all devices. We discuss the possible connection between isosteric heats (and binding energies), the nanotube type and radius, and a recent grand canonical Monte Carlo (GCMC) calculation of the adsorption of Kr and Ar on a zigzag ($n, m = 18, 0$) and an armchair (12, 12) nanotube [10].

2 Experimental

After several fabrication steps, a suspended nanotube resonator consists of a single-walled carbon nanotube grown *in situ* across a trench 1 or 2 μm wide on an oxidized silicon wafer. Previously deposited Pt electrodes on the edges of the trench serve as source and drain. A third Pt electrode deposited on the bottom of the trench is used as a gate. The nanotube may be semiconducting or metallic depending on its diameter and chirality. For semiconducting nanotubes, the device acts as a field-effect transistor. To determine the nanotube type we measure its source-drain conductance, G, as a function of gate voltage V_g. We detect a resonance frequency, f_{res}, using the so-called mixing technique [11–13]. A signal at radio frequency f in the range 10 MHz to 500 MHz, modulated at $\delta f = 1$ kHz, is applied to the source and the resulting current component at δf is detected using a current amplifier and a lock-in detector referenced to δf. At resonance this "mixing current" shows a feature produced by the nonlinearity due to the changing gate capacitance as the nanotube vibrates with an enhanced amplitude.

For isotherm measurements V_g is chosen to obtain the clearest possible resonance, the temperature is set, and a narrow sweep of f around f_{res} is done for the bare nanotube and as the pressure in the chamber is incremented in small steps. Adsorption increases the mass per unit length of the nanotube, which lowers f_{res}. The result is an isotherm of f_{res} vs. P at given T. To convert f_{res} to a measure of mass adsorbed (the "coverage", ϕ) we assume f_{res} is inversely proportional to the square root of the mass of the nanotube plus adsorbate. This is correct if the adsorbate is uniformly

distributed and the vibrations are linear, and it turns out to work surprisingly well. With this assumption the coverage is given by

$$\phi = N_{ads}/N_C = (M_C/M_{ads})\big[(f_0/f_{res})^2 - 1\big], \tag{1}$$

where N_{ads}/N_C is the ratio of the number of adsorbed atoms to carbon atoms, M_C and M_{ads} are the molecular weights of carbon and adsorbate, and f_0 and f_{res} are respectively the resonance frequencies of the bare nanotube and of the nanotube plus adsorbate. With this definition the commensurate structure formed by Kr and ^{4}He on graphite, where 1/3 of the graphite hexagons are occupied by an adsorbate atom, corresponds to $\phi = 1/6 = 0.167$. The number density measured by low energy electron diffraction (LEED) of a Kr/graphite monolayer at 47 K is $n \approx 0.072$ Å^{-2} [14] when a second layer forms, almost equal to the density of (111) planes of 3d Kr at the same T [15]. For ^{4}He/graphite, estimated monolayer densities from heat capacity measurements are $n \approx 0.115$ Å^{-2} at 5 K [16] and $n \approx 0.120$ Å^{-2} below 2 K [17], which correspond to $\phi_{Kr} \approx 0.186$ and $0.301 < \phi_{He} < 0.315$. On a nanotube of radius R, where a uniform monolayer will be at a distance d_s from the substrate, a monolayer of the same two-dimensional density as one on graphite will have a coverage larger by the ratio of radii, $(R + d_s)/R$. Thus for Kr on a $R = 1$ nm nanotube, with $d_s \approx 0.35$ nm the maximum possible monolayer coverage will be $\phi_{Kr,max} \approx 0.25$.

The conductance G was measured using a low frequency (typically 740 Hz) AC source-drain excitation V_{sd} comparable with $k_B T/e$, with V_g set at a value near zero where G is highly sensitive to changes in V_g. G responds to changes in the density of the adsorbate (see next section).

The silicon chip with the device is wire-bonded into a 14-pin dual-in-line package. This in turn plugs into a socket mounted inside a vacuum chamber (about 100 cc volume) connected to a room temperature vacuum and gas dosing system with three capacitance gauges having ranges of 0.250, 10 and 1000 Torr and hermetic wire feedthroughs. An oil-free turbomolecular pump cart provides the vacuum. The vacuum chamber can be submerged in a liquid nitrogen bath whose temperature T can be changed over a small range (68 K to 77.4 K), our initial setup, or attached to a mechanical cryocooler with a range of 4.3 K to 350 K. The pressure in the chamber is obtained by applying a thermo-molecular correction to that measured by the room temperature gauges, using the empirical data and equation from Takaishi and Sensui [18]. Devices are easily destroyed during T and P cycling, quite likely because of contaminants solidifying on them; thus we did not manage to obtain complete sets of isotherms for each device with both gases.

3 Results

3.1 Krypton

Figures 1–3 show coverage isotherms for three devices. The first set, for YB8 (Fig. 1), were measured in the liquid nitrogen cryostat. In each isotherm there is one large riser, too sharp to be resolved with the pressure intervals used, followed by a smaller, smoother riser in the range $0.18 < \phi < 0.19$. It is natural to interpret the large riser
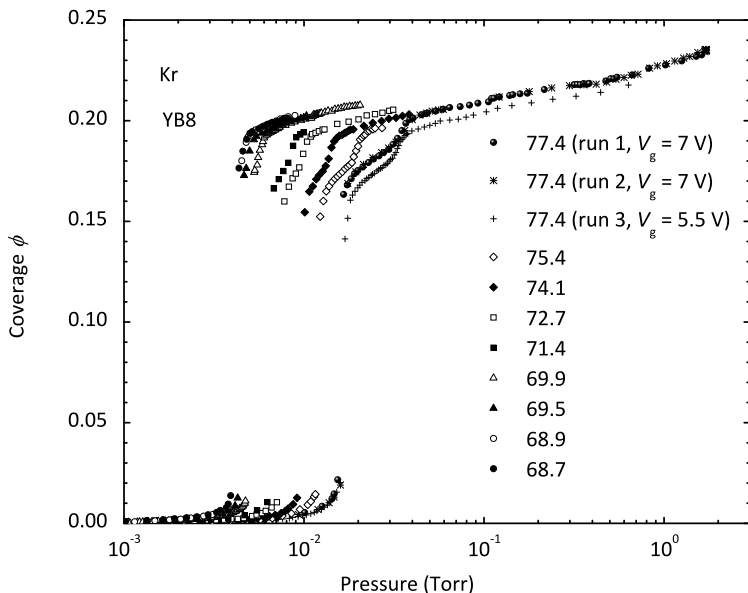
Fig. 1 Kr coverage isotherms on device YB8 obtained using resonance frequency measurements. Notice the large steps, vertical within the experimental resolution, for $0.01 < \phi < 0.17$, and smaller smoother increase near $\phi \approx 0.19$, which moves to higher P with higher T. One can interpret the larger jump as a vapor-liquid transition and the smaller jump as the liquid-incommensurate solid transition (see text). The isotherms at 77.4 K extend to the Kr saturated vapor pressure of 1.75 Torr at which ϕ reaches a maximum of 0.23

as the Kr vapor–liquid (V–L) transition since the size of the large jump increases as T is lowered, and the smaller one as a liquid–solid (L–S) transition (where we do not know whether the solid is commensurate or not). The maximum coverage that can be attained, which is limited by the Kr 3d saturated vapor pressure of $P_{vapor} = 1.75$ Torr that is reached in two of the 77.4 K isotherms, is about 0.24. This value is of the order of the estimated $\phi_{Kr,max}$ for a 1-nm radius nanotube if the Kr surface density was the one of Kr/graphite, which we don't expect it to be due to reduced attraction to the substrate [10]. Once P_{vapor} is reached it is impossible to build a second layer. There is a small shift in ϕ in the third isotherm at 77.4 K which reflects the uncertainties in reproducing an isotherm after several cycles.

Devices YB10a (Fig. 2) and YB12 (Fig. 3) were measured using the cryocooler. Surprisingly, the pressures at the large risers in the 70 K isotherms for these two devices are an order of magnitude higher than for YB8 at the same T. Also, in the case of YB10a, the riser is clearly not vertical. The maximum coverage ϕ_{max} is about 0.09 for YB10a and 0.15 for YB12, both well below the value for YB8.

Figure 3 shows isotherms of the conductance G for YB12 at 60 K, 65 K and 70 K, measured at the same time as the coverage isotherms. Relatively sharp risers in the conductance always coincide with those in ϕ, and can therefore be used as an alternative means to detect the phase transitions. However, the variation in G between runs and the lack of a theory to connect conductance changes with temperature and
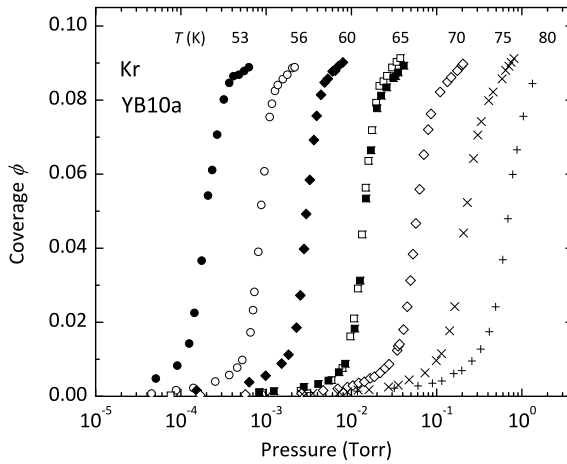
Fig. 2 Kr isotherms on device YB10a at $V_g = 3$ V. The maximum ϕ reached is only 0.09. The isotherm at 65 K was measured at $V_g = 1.5$ V (*open squares*) and 4.0 V (*solid*), which produced a small difference in the resonance frequency reflected in the coverage calculated using Eq. (1). In this device the isotherms at the presumed vapor-liquid step are not vertical
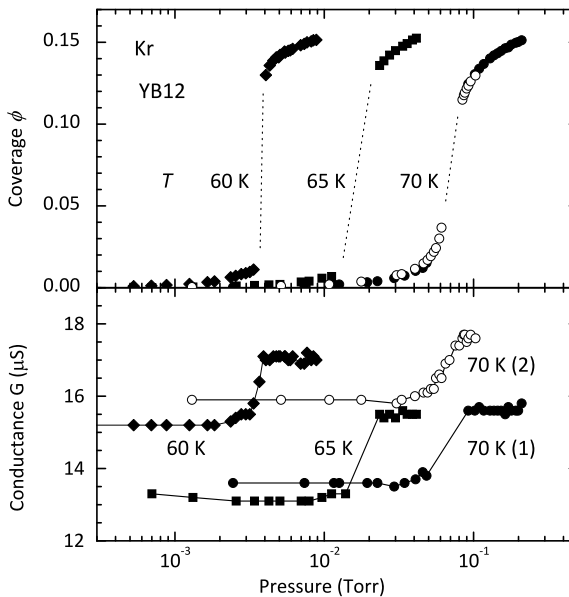

Fig. 3 Coverage (*top panel*) and conductance (*bottom panel*) isotherms measured at the same temperatures on the same device, YB12. The conductance varies somewhat on cycling T or P which is why the vertical position of the G isotherms is variable

adsorbate density make the G isotherms, for now, useful only for detecting sudden density changes due to phase transitions.
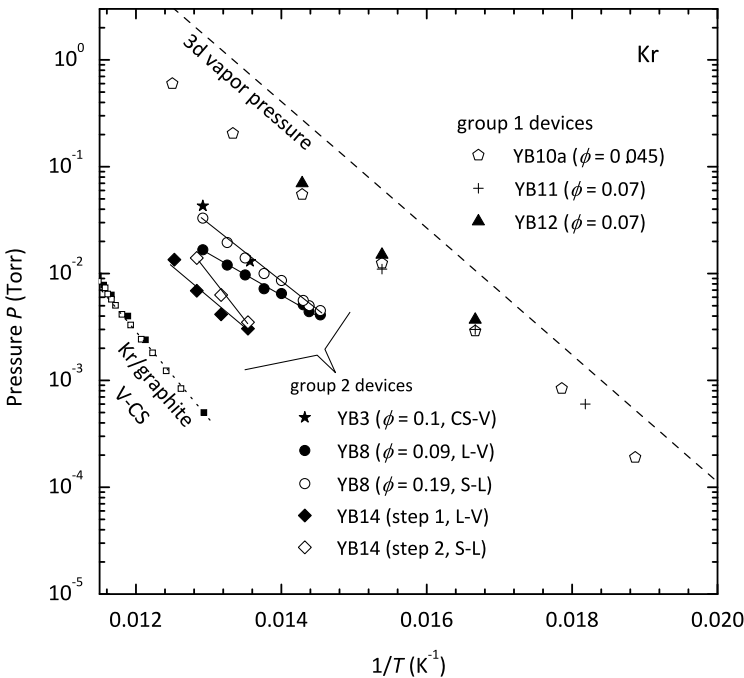
Fig. 4 Log P vs. $1/T$ for Kr on several devices. Also shown are the vapor pressure of Kr at the sublimation line (S–L phase coexistence) and the CS–V coexistence line of Kr adsorbed on graphite (*black squares*, Ref. [19]; *white*, Ref. [20]). Where vertical jumps are observed, as for YB8 and YB14, *solid straight lines* have been drawn through the data. From these we can extract apparent positions of S–L–V triple points in the surface phases

In Fig. 4 we plot on a log P vs. $1/T$ graph the positions of the risers for these devices plus three others where we obtained meaningful data. The measurements on YB14 were obtained purely from conductance isotherms. Figure 4 shows also the positions of the V–CS (commensurate solid) phase transition of Kr on graphite from the literature [3, 19, 20], and of the Kr 3d V–S transition (P_{vapor}). Where there are clear phase transition jumps (large vertical step at low P and smaller jumps at higher P on the same isotherm for YB3, YB8 and YB14) we have drawn straight lines representing the V–L and L–S phase boundaries. We do not distinguish between commensurate and incommensurate solid (IS).

The devices appear to fall into two groups. YB10a, YB11, and YB12 have similar behavior to each other, with higher vapor pressures on adsorption, translating to a lower surface binding energy. Only three isotherms were measured on YB11, at 60, 65 and 70 K, before the device failed. None of these devices attains the expected coverage of a full monolayer when the 3d Kr vapor pressure is reached. For YB10a, $\phi_{max} \approx 0.09$, for YB11 $\phi_{max} \approx 0.14$, and for YB12, $\phi_{max} \approx 0.15$ to 0.16. As shown in Fig. 5, at 60 K these three devices yield essentially the same vapor pressure at the middle of the large riser at half coverage, $P \approx 3 \times 10^{-3}$ Torr, but the slope of the step increases with ϕ_{max}. Broadening of an L–V step is conventionally related to inhomogeneities or finite size effects.
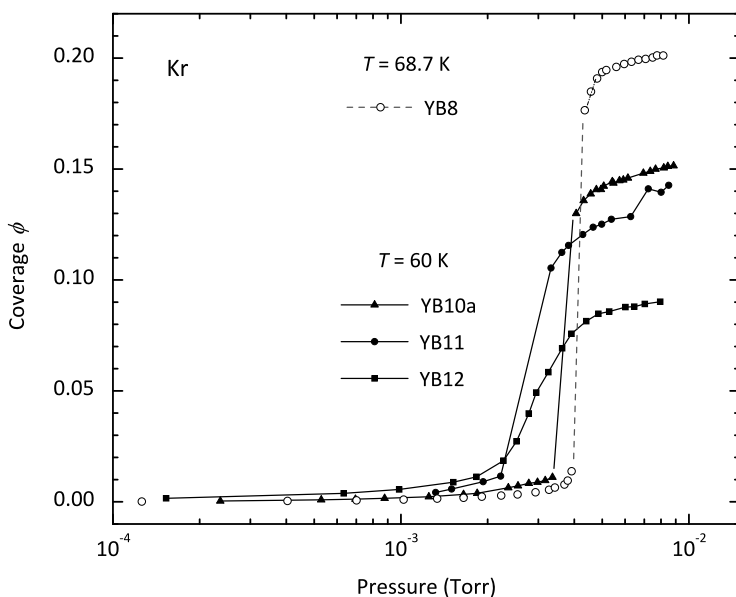
Fig. 5 Four isotherms obtained at comparable equilibrium pressures. The YB10a, YB11 and YB12 isotherms were all measured at $T = 60$ K, while the YB8 isotherm was measured at 68.7 K. For YB8 the higher temperature of the isotherm for a comparable pressure at the step indicates stronger binding than on the other three devices. In addition for YB8 the maximum coverage approaches the one expected for a 2 nm diameter nanotube and a solid close-packed Kr monolayer, while for the others it is lower

Devices YB3, YB8, and YB14 form the second group with similarities to each other (see Fig. 4) with equilibrium vapor pressures lower than for the YB10a group. We show in Fig. 5 that the step at comparable P for YB8 occurs at a higher T than for YB10a, YB11 and YB12, and it achieves $\phi_{max} \approx 0.2$. The Kr isotherm at 77.4 K on YB3 shown in Fig. 3 of Ref. [9] has a vertical jump from small ϕ up to $\phi \approx 0.16$, close to the CS coverage on graphite, and at least two more transitions at higher coverage before reaching $\phi_{max} \approx 0.23$ at P_{vapor}. YB8 and YB14 have both L–V and S–V transitions.

The measurements on YB14 indicate that the L–V critical temperature, at which the monolayer loses the vertical step (the end point of an infinite 2d isothermal compressibility), is about 77.9 K. Although for YB8 we could not go above 77.4 K, its L–V critical point T_c is close to 80 K as estimated from the decrease in the magnitude of the larger vertical step (the coexistence region), see Fig. 1. The S–V and L–V lines in Fig. 4 converge to what should be the S–L–V triple point. For YB8, $T_t \approx 68$ K, slightly below the lowest measured temperature. For YB14, $T_t \approx 73$ K, also below the lowest measured temperature. The differences between these two devices is likely real, but may be due to inaccuracy in the low P measurements and the thermo-molecular corrections in the two different experimental setups. We cannot determine the L–V and S–L–V critical and triple temperatures for YB10a, YB11, and YB12, if indeed they exist.
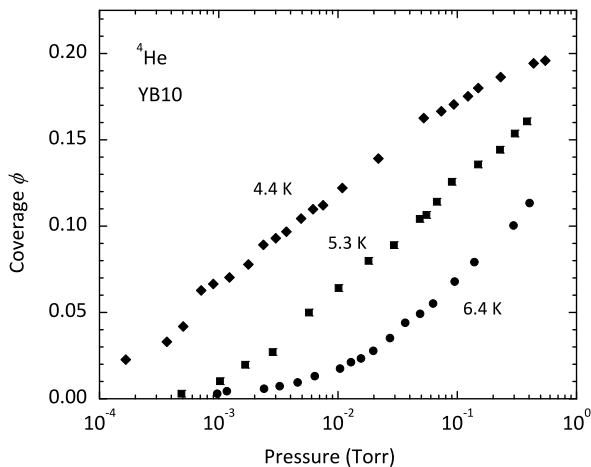
Fig. 6 Three helium coverage isotherms using resonance frequency measurements on device YB10 (a different device from YB10a)

3.2 Helium

Figure 6 shows three ^{4}He isotherms obtained from resonance frequency measurements on device YB10 at 4.4 K, 5.3 K, and 6.4 K. Device YB10 was fabricated in the same batch as device YB10a, but it is not the same. We show in Fig. 7 the pressure and temperature at the middle points of the isotherms of ^{4}He on YB10 and YB14 (measured only using conductance, see below) in a log P vs. $1/T$ diagram. For comparison we also show results derived from volumetric isotherms of ^{4}He on graphite measured (and thermo-molecular corrected) by Elgin and Goodstein [21, 22] over a similar range of temperatures, and the vapor pressure of liquid ^{4}He up to its 3d boiling temperature at 760 Torr, 4.2 K. We see that for equal T, the ^{4}He monolayer equilibrium pressures are higher on YB10 than on YB14, and are higher on both than on graphite, as was the case with Kr.

Our isotherms are measured at much higher T than the two-dimensional (2d) L–V critical point of ^{4}He, which is at about 0.9 K [23, 24], and also well above the highest T of its CS–F transition on graphite, 3 K [2]. The lowest density of the 2d L–S transition on graphite measured for ^{4}He is 0.079 Å^{-2} ($\phi \approx 0.21$) at 1 K, and the solid melting line density at 4.4 K is 0.102 Å^{-2} ($\phi \approx 0.27$), so isotherms on YB10 did not reach the high coverage or low temperature needed to observe a phase transition [2, 3, 15, 21].

The results on YB14 in Fig. 7 were obtained from conductance measurements alone. At these low temperatures there are Coulomb blockade peaks in G as a function of V_g which lead to complications in the conductance isotherms. We then employed a method slightly different to that described in the experimental section: rather than fixing V_g, we tracked the value of V_g associated with a given Coulomb blockade peak as a function of P. The result is similar.
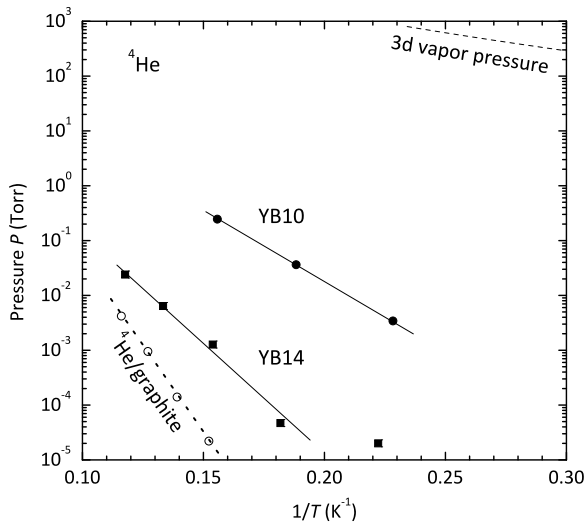
Fig. 7 Log P vs. $1/T$ for ^{4}He. Included in the graph are the 3d vapor pressure of liquid ^{4}He up to its critical point and the P and T values obtained from isotherms on ^{4}He/graphite measured by R.L. Elgin (PhD Dissertation, Table I Appendix) [22]

4 Further Analysis and Discussion

From adsorption isotherms such as those shown in the previous section one can calculate the isosteric (constant coverage) heat of adsorption, which is given (in units of temperature) by

$$Q_{\mathrm{st}} = -\left[\partial \ln P / \partial (1/T)\right]\big|_{\phi} \tag{2}$$

at each value of the coverage. Results for Kr are shown in Fig. 8 for all the devices from which more than two isotherms were obtained. For YB14, whose behavior is similar to YB8, we mapped the steps in G onto the steps in ϕ at the S–L transition in YB8. Thus, although their Q_{st} magnitudes are quite different in other ways they behave similarly. We have indicated in Fig. 8 the latent heat of fusion of 3d Kr, and the Q_{st} of Kr adsorbed on exfoliated graphite at the CS–V coexistence (the slope of the Kr/gr line in Fig. 4, from volumetric isotherms [19, 20]). A complete review of the many phases found for Kr/gr has been published by Specht et al. [25], summarized in Ref. [3].

The Q_{st} values we obtain are lower than those for Kr/gr. Q_{st} shows significant variations between devices. Having preliminary results from only two devices, we have not made a graph similar to Fig. 8 for our ^{4}He isotherms. However, Fig. 7 shows that for ^{4}He on devices YB10 and YB14, the slopes of lines drawn by eye through the available points yield Q_{st} considerably lower than on graphite in the same temperature interval and for similar coverage at about the middle of the hypercritical fluid: 146 K for adsorption on graphite, between 66 and 72 K for YB14, and about 50 K from the three isotherms on YB10, less than half the Q_{st} on graphite. Such a large decrease seems plausible because for ^{4}He the binding is significantly reduced by a
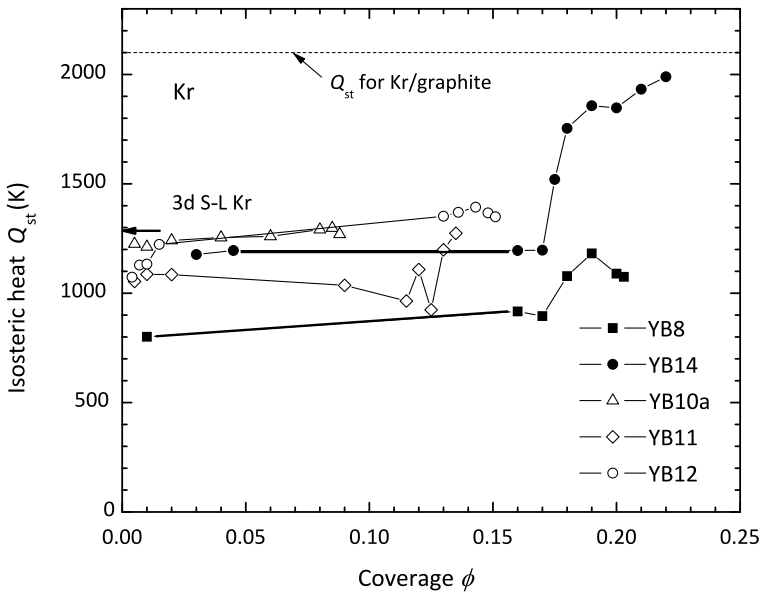
Fig. 8 Isosteric heat of adsorption of Kr for five devices as a function of coverage. The coverage for device YB14, which was measured with conductance isotherms only, was assumed to match that of YB8 at $\phi = 0.19$. The *thick solid lines* indicate the vertical risers in YB8 and YB14

large zero point energy. This suggests that nanotubes may present an alternative system to the alkali metals [5, 6] for studying superfluid monolayers. It may turn out to be impossible to reach the S–F transition above the L–V critical point, in which case one could have a continuous fluid monolayer for nanotubes which are strong enough adsorbers to hold a monolayer but that cannot reach the surface density needed for compression of the monolayer into a solid.

Kim et al. [10] have modeled the adsorption of Kr on individual single-walled nanotubes using the GCMC technique, obtaining theoretical adsorption isotherms between 60 K and 100 K, a temperature range similar to ours. For a zigzag $(18, 0)$ nanotube they find isotherms exhibiting an L–V transition, with a $T_c \approx 100$ K, and for an armchair $(12, 12)$ nanotube they find $T_c \approx 95$ K. We determined the L–V T_c to be ≈ 80 K on devices YB8 and YB14. Apparent 2d L–V critical points of Kr on a variety of substrates, including MgO, are in the range of 75 K to 90 K (see Table I of Coulomb et al. [26]). Kim et al. attribute the difference between their calculation and the theoretical 2d T_c of 89 K for a pure 2d Lennard-Jones system to possible substrate screening effects. Interestingly though, Kim et al. find at their lowest temperatures that commensurate structures are formed at $\phi = 1/4$ and $1/6$. Previously [9] we found evidence that for device YB3 the $1/6$ commensuration was realized. Kim et al.'s calculations indicate that this is possible only for (n, n) nanotubes with $n > 19$, which would correspond to a large nanotube diameter of 3.6 nm, very unlikely to be realized in our experiment. For the $(n, 0)$ zigzag nanotubes a $1/4$ CS striped structure is favored for $n < 15$, a triangular CS is favored for $15 < n < 40$, and the $1/6$ CS is favored for $n \geq 40$.

The different CS structures occur because of the increasing nanotube diameter with n which eventually allows the formation of the 1/6 CS corresponding to that formed by Kr on graphite. Since we do not know the nanotube diameter or chirality in our devices we cannot comment on the accuracy of the GCMC calculations. The only nanotube devices for which ϕ reaches ≈ 0.24, approximately one full monolayer, are YB3 and YB8. It is likely that YB14 also goes to that coverage, but we do not have a way of converting conductance to coverage. In YB8 (Fig. 1) our liquid coverage goes up to $\phi \approx 0.18$ at T_t. In Kim et al. the liquid coverage is $\phi \approx 0.23$. These differences may be due to a problem with converting f_{res} to ϕ using Eq. (1), but the measurements on YB8 and YB14 clearly show that Kr on these devices has a triple point. Further calculations in the region of the estimated S–L–V triple point would be very useful.

Kim et al. also calculated the gas-gas (E_{gg}), gas-substrate (E_{gs}) and total energies for adsorption on the (18, 0) and (12, 12) nanotubes for both a smooth substrate approximation [27] and including the individual carbon atoms, using several potentials. The total energy, E, per adsorbed atom, in units of temperature, is given by

$$E = E_{gs} + E_{gg} = -Q_{st} + \alpha T, \tag{3}$$

where α is a numerical factor which depends on the monolayer phase, being between 1/2 and 3/2. E_{gs} is a function of the nanotube radius. Using the smooth substrate approximation we calculated numerically that at the minimum potential above the surface E_{gg} will vary between -960 K for a 0.5 nm radius nanotube and $-1{,}210$ K for infinite radius (i.e., a graphene sheet). The (18, 0) and (12, 12) nanotubes used in Ref. [10] have similar radii of 0.70 and 0.81 nm, which for a smooth substrate gives $E_{gs} \approx -1{,}100$ K at the minimum of the potential. The values of E in Ref. [10] are quite similar for the two types of nanotubes, at roughly $-1{,}600$ K. Using this value of E, an average isotherm temperature of 70 K, and $\alpha = 1.5$ in Eq. (3), we can then estimate from their calculations that the Q_{st} measured at the solid monolayer completion should be around 1,700 K. Device YB14 (Fig. 8) yields a Q_{st} close to this value at monolayer completion, but none of the other devices do. Although device YB8 has the expected variation of Q_{st} with coverage, we can not explain its rather low value.

Finally, close examination of Fig. 4 shows that an extrapolation of the S–L coexistence line of YB14 to lower temperatures will diverge from the sublimation line of 3d Kr, but the same extrapolation for YB8 will be either parallel to or run into the Kr vapor pressure at some low temperature. While not drawn on the plot, an extrapolation of the data for YB10a, YB11 and YB12 at the middle of the step converges towards the 3d vapor pressure. Monolayer coexistence lines, or equal coverage lines, running into the 3d vapor pressure line means that Kr will only partially wet the substrate. This is consistent with the formation of only a partial monolayer for these devices.

5 Summary

We have reported quantitative measurements of the adsorption of Kr and ^{4}He on individual single wall carbon nanotubes. Both the resonance frequency measurements and the conductance measurements yield good isotherms. For some of the devices

we observe phase transitions in the Kr isotherms using both techniques. The lower binding energy on nanotubes allows us to measure isotherms at lower temperatures than on graphite. We obtained values for what seem to be the L–V critical and S–L–V triple temperatures of Kr by using the data on two devices, YB8 and YB14. The low binding energy of ^{4}He on nanotubes, and the great uniformity of the nanotube surface for at least some devices, bode well for measuring first-monolayer adsorption isotherms of both helium isotopes on this unique substrate down to the 1 to 2 K range in the near future.

References

1. D.M. Young, A.D. Crowell, *Physical Adsorption of Gases* (Butterworths, Stoneham, 1962)
2. J.G. Dash, *Films on Solid Surfaces* (Academic Press, San Diego, 1972)
3. L.W. Bruch, M.W. Cole, E. Zaremba, *Physical Adsorption: Forces and Phenomena* (Oxford University Press, London, 1997)
4. A.D. Migone et al., Phys. Rev. B **31**, 7643 (1985)
5. P. Taborek, J.E. Rutledge, Phys. Rev. Lett. **71**, 263 (1993)
6. P. Taborek, J. Low Temp. Phys. **157**, 101 (2009)
7. A. Velasco, F. Huisman, E. Van Cleve, P. Taborek (2012), http://meetings.aps.org/link/BAPS.2012.MAR.H16.4
8. G. Zimmerli, M.H.W. Chan, Phys. Rev. B **45**, 9347 (1992)
9. Z. Wang et al., Science **327**, 552 (2010)
10. H.-Y. Kim, M.W. Cole, M. Mbaye, S.M. Gatica, J. Phys. Chem. A, Mol. Spectrosc. Kinet. Environ. Gen. Theory **115**, 7249 (2011)
11. V. Sazonova et al., Nature **431**, 284 (2004)
12. J. Cao, Q. Wang, D.W. Wang, H.J. Dai, Small **1**, 138 (2005)
13. J. Chaste, A. Eichler, J. Moser, G. Ceballos, R. Rurali, A. Bachtold, Nat. Nanotechnol., published online 01 April 2012
14. S.C. Fain Jr., M.D. Chinn, J. Phys., Colloq. **38**, C4-99 (1977)
15. G.L. Pollack, Rev. Mod. Phys. **36**, 748 (1964)
16. M. Bretz, J.G. Dash, D.C. Hickernell, E.O. McLean, O.E. Vilches, Phys. Rev. A **8**, 1589 (1973)
17. D.S. Greywall, Phys. Rev. B **47**, 309 (1993)
18. T. Takaishi, Y. Sensui, Trans. Faraday Soc. **59**, 2503 (1963)
19. A. Thomy, X. Duval, J. Chim. Phys. **67**, 1101 (1970)
20. Y. Larher, J. Chem. Soc. Faraday Trans. I **70**, 320 (1974)
21. R.L. Elgin, D.L. Goodstein, Phys. Rev. A **9**, 2657 (1974)
22. R.L. Elgin, PhD dissertation, Caltech, 1973 (unpublished)
23. P.S. Ebey, O.E. Vilches, J. Low Temp. Phys. **101**, 469 (1995)
24. M.C. Gordillo, D.M. Ceperley, Phys. Rev. B **58**, 6447 (1998)
25. E.D. Specht et al., Z. Phys. B, Condens. Matter **69**, 346 (1987)
26. J.P. Coulomb, T.S. Sullivan, O.E. Vilches, Phys. Rev. B **30**, 4753 (1984)
27. G. Stan, M.W. Cole, Surf. Sci. **395**, 280 (1998)